Colloids and Surfaces B: Biointerfaces 87 (2011) 109–115

Contents lists available at ScienceDirect

Colloids and Surfaces B: Biointerfaces

journal homepage: www.elsevier.com/locate/colsurfb

Bacterial adhesion on hybrid cationic nanoparticle–polymer brush surfaces: Ionic strength tunes capture from monovalent to multivalent binding

Bing Fang[a], Saugata Gon[b], Myoung Park[c], Kushi-Nidhi Kumar[d], Vincent M. Rotello[c], Klaus Nusslein[d], Maria M. Santore[a,*]

[a] Department of Polymer Science and Engineering, University of Massachusetts at Amherst, Amherst, MA 01003 USA
[b] Department of Chemical Engineering, University of Massachusetts at Amherst, Amherst, MA 01003 USA
[c] Department of Chemistry, University of Massachusetts at Amherst, Amherst, MA 01003 USA
[d] Department of Microbiology, University of Massachusetts at Amherst, Amherst, MA 01003 USA

ARTICLE INFO

Article history:
Received 18 January 2011
Received in revised form 4 April 2011
Accepted 3 May 2011
Available online 10 May 2011

Keywords:
Poly(ethylene glycol)
PEG
Poly(ethylene oxide)
PEO
Bacterial adhesion
Bacterial attachment
Functionalized brush
Nanoparticle-bacterial interactions
Biofouling

ABSTRACT

This paper describes the creation of hybrid surfaces containing cationic nanoparticles and biocompatible PEG (polyethylene glycol) brushes that manipulate bacterial adhesion for potential diagnostic and implant applications. Here, ~10 nm cationically functionalized gold nanoparticles are immobilized randomly on negative silica surfaces at tightly controlled surface loadings, and the remaining areas are functionalized with a hydrated PEG brush, using a graft copolymer of poly-l-lysine and PEG (PLL–PEG), containing 2000 molecular weight PEG chains and roughly 30% functionalization of the PLL. The cationic nanoparticles attract the negative surfaces of suspended *Staphylococcus aureus* bacteria while the PEG brush exerts a steric repulsion. With the nanoparticle and PEG brush heights on the same lengthscale, variations in ionic strength are demonstrated to profoundly influence the capture of *S. aureus* on these surfaces. For bacteria captured from gentle flow, a crossover from multivalent to univalent binding is demonstrated as the Debye length is increased from 1 to 4 nm. In the univalent regime, 1 um diameter spherical bacteria are captured and held by single nanoparticles. In the multivalent regime, there is an adhesion threshold in the surface density of nanoparticles needed for bacterial capture. The paper also documents an interesting effect concerning the relaxations in the PLL–PEG brush itself. For brushy surfaces containing no nanoparticles, bacterial adhesion persists on newly formed brushes, but is nearly eliminated after these brushes relax, at constant mass in buffer for 12 h. Thus brushy relaxations increase biocompatibility.

1. Introduction

Bacterial adhesion to plastic and metal surfaces contributes to the spread of hospital infections and, inside the body, leads to biofouling and contamination that results in device failure, for instance in catheters, IV needles, and implants. The study of bacterial adhesion to polymer surfaces and the design of antimicrobial surfaces therefore constitute large research areas with continued growth. Our interest lies in the development of smart surfaces with the potential for precisely tuned selective bacterial adhesion, for instance for rapid diagnostics. We also envision surfaces which could be further refined for selective bacterial killing without harming mammalian cells or desirable types of bacteria. These goals require precise control of bacterial adhesion itself, particularly the initial steps, at the focus of the current paper.

Two classes of surfaces, developed for bacterial manipulation, are hydrated brushes and cationic surfaces. The hydrated brushes are often comprised of polyethylene glycol (PEG) [1,2]. Depending on their architecture and surface attachment chemistry, they eliminate bacterial adhesion to different extents. Some labs report reduced bacterial adhesion on end-tethered PEG surfaces [1,3–6] while others report that it is almost entirely eliminated [7–10]. Some report substantial differences in the bacterial types which can adhere on PEG brushes [7,11–13] while commercial cross-linked PEG coatings have been shown to reduce bacterial colonization in short-term in vivo experiments [14]. However, only a few labs have focused on how systematic variations in PEG brush architectures influence bacterial adhesion. Here, as with PEG brush resistance to protein adsorption, the key is the formation of an appropriately thick PEG corona that prevents access to electrostatic and van der Waals interaction with the substrate, at the same time ensuring sufficient anchoring chemistry at the base of the PEG brush [1,7–9,13,15].

* Corresponding author.
E-mail address: santore@mail.pse.umass.edu (M.M. Santore).

0927-7765/$ – see front matter © 2011 Elsevier B.V. All rights reserved.
doi:10.1016/j.colsurfb.2011.05.010

Numerous cationic surfaces have been developed to kill bacteria on contact without leaching compounds. A problem, however, with the cationic-contact surfaces is their tendency to foul with serum proteins or with bacterial products, reducing anti-microbial effectiveness [16]. Recent studies, therefore have sought hybrid surfaces with cationic character and controlled adhesion. In a recent example, mixed brushes of PEG and P2VP (poly (2-vinyl pyridine)) demonstrate a large range of tunability in bacterial adhesion, through the covalent attachment of different relative amounts of end-reactive polymers [17]. While micropatterning of adhesive regions in a PEG brush has proven useful in the development of bacterial arrays, [18–20] Zydrko [17] suggests that heterogeneity on smaller lengthscales could prove versatile for manipulating the average bacterial interactions with surfaces, a concept we pursue here through a new hybrid surface that combines cationically functionalized gold nanoparticles (order 10 nm in diameter) with a PEG brush. While these cationic nanoparticles may be harmful to bacteria (a desirable property which we consider further in future work), in this work they drive bacterial adhesion on macroscopic surfaces. Cationic nanoparticles are also chosen here because their combined electrostatic and van der Waals attractions (especially involving the gold core) to the substrate make their deposition practically irreversible [21].

This paper introduces a PEG-brush nanoparticle hybrid surface, in Fig. 1, and describes its fabrication and provides characterization with AFM and reflectometry. This paper follows a protein adsorption study on a related but different surface comprising flat cationic polymer patches embedded at the base of a similar PLL–PEG brush [22]. The current paper, in which the nominal ~10 nm nanoparticles protrude from the surface well into the brush, then examines the key features of bacterial adhesion on these surfaces. *Staphylococcus aureus* was chosen as a model organism because of its direct relevance to hospital and device infections [23,24]. *S. aureus* is a 1-um sphere with negative charge, somewhat resembling 1-um silica spheres in our prior work [25–28]. The influence of ionic strength on bacterial adhesion is studied and it is demonstrated how ionic strength can be used to tune a mechanistic crossover in bacterial adhesion from univalent to multivalent cell capture. The adhesive mechanism with the nanoparticle hybrid surface is compared with that operating in a model system based on 1-um spheres resembling the *S. aureus* bacteria. Fundamental differences between surfaces dominated by steric repulsive forces and those dominated by background electrostatic repulsions are described. Also, a peripheral observation is reported: relaxations in the PEG brush increase bacterial resistance with brush aging time (at fixed interfacial mass), an effect not previously documented to our knowledge.

2. Experimental details

Cationically functionalized gold nanoparticles were synthesized with overall diameters near 11 nm, measured by TEM in the dry state. The 11 nm particles were grown from 7 nm gold cores with a shell of roughly 500 ligands, 200 of which were *N*,*N*,*N*-trimethyl (11 mercaptoundecyl) ammonium chloride ligands. The other 300 ligands were 1-mercaptoundecane molecules [29,30].

The "backfill" brush was a PLL–PEG graft copolymer, having 2300 molecular-weight PEG side arms, a 20,000 molecular weight PLL backbone, and a grafting ratio [31,32] of 2.9 ± 0.1, meaning there were 2.9 PLL units per each PEG arm, or a PLL functionalization of 34%. This graft copolymer was synthesized according to the method of Hubbell and Textor [31,32], using a 50 mM solution of PLL in borate buffer to which the *N*-hydroxysuccinimidyl ester of methoxypoly(ethylene glycol) acetic acid (Laysan Bio Inc.) was added. After reaction for 6 h, dialysis against pH 7.4 phosphate buffer (0.008 M Na_2HPO_4 and 0.002 M KH_2PO_4, total ionic strength $I = 0.026$ M) followed by dialysis against DI water yielded the product which was stored at −20C after freeze drying. ^{1}H NMR analysis of the polymer dissolved in D_2O, using a Bruker 400 mHz instrument allowed the areas of the lysine side chain peak (–CH_2–N–) at 2.909 ppm and the PEG peak (–CH_2–CH_2–) at 3.615 ppm to be compared to determine the grafting ratio.

Silica substrates were microscope slides (FisherFinest, Fisher, Inc.) subject to overnight soaking in concentrated sulfuric acid, shown to remove metal cations and produce a relatively smooth silica surface. Following a thorough rinse with DI water, slides were placed in a slit shear flow chamber, and exposed to flowing buffer. Then following a valve turnover, a 5 ppm nanoparticle solution in DI water was flowed over the surface. Nanoparticle deposition was roughly linear in time, especially at short times when the surface was sparse with nanoparticles, per our interests. Continued flow for tightly controlled exposure times produced surfaces with randomly deposited nanoparticles of highly controlled densities. After the desired deposition period, DI water was reinjected into the chamber to flush nanoparticles from the bulk. Phosphate buffer was then introduced, and once the flow chamber had been thoroughly flushed, a 100 ppm PLL–PEG solution was introduced and allowed to flow for 10 min, to ensure surface saturation around the nanoparticles. At this point flow was switched back to buffer. Next, in most cases, the chambers were dissembled and substrates stored in phosphate buffer for 12 h prior to their re-insertion in the flow chamber and bacterial studies. This surface aging step was necessary, as we show below, to obtain a fully relaxed brush.

When the deposition of the nanoparticles or polymer was tracked kinetically, near-Brewster optical reflectometry was employed. This method is similar to ellipsometry, but by using a parallel-polarized HeNe beam impinging on the interface near the Brewster from behind the solid substrate, glass substrates could be accommodated. At the Brewster angle of a perfect interface there is no back-reflected beam. However, when small amounts of a material accumulate on a surface, the back-reflection grows as the square of the adsorbed mass.

A Multi-Mode AFM-2 with a Nanoscope IV scanning probe microscopy controller (Veeco Instruments, Inc.) was used for imaging. Standard tapping mode AFM probes with nominal spring constants of 42 N/m and nominal resonance frequencies of 320 KHz were employed. Imaging was carried out in tapping mode with RMS amplitudes between 0.5 and 1.0 V. Scan rates of 1 Hz were used. Captured images were processed offline using Nanoscope 5.12r2 software (Veeco, Inc.). Images were flattened using a 1st order flattening function. The particle analysis tool in the software was used to determine particle heights.

AFM micrographs were obtained on bare acid-etched microscope slides in a dry state after deposition of nanoparticles (and brush polymer) via the flow system used in the reflectometry experiments. The substrates, functionalized nanoparticles and PLL–PEG brush polymer used were identical to those used in the reflectometry experiments. Samples were removed from the flow cell under a continuous stream of Milli-Q (Millipore, Inc.) filtered de-ionized water (18 MΩ impedance) after deposition. Samples were subsequently dried in an ambient laboratory condition prior to imaging.

Per standard procedures, *S. aureus* bacteria (ATCC 25923) were grown in Luria-Bertani (LB) medium. The cultures were incubated aerobically overnight at 37 °C, with shaking at 200 rpm and harvested after a total of 24 h during logarithmic growth. Protein and other molecules which might potentially contaminate the surfaces were removed from bacterial suspensions by centrifugation at $1000 \times g$ and cells re-suspended in phosphate buffer, a procedure which was conducted twice. The final bacteria concentration for adhesion studies was 5×10^5 cells/ml. All bacteria were used

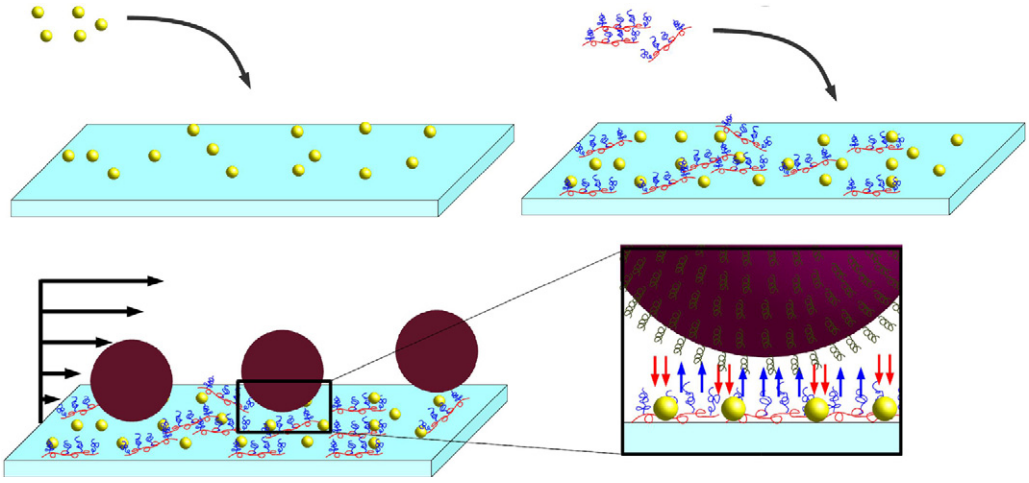

Fig. 1. Hybrid surface containing cationically functionalized nanoparticles, subsequently backfilled with a graft copolymer brush. With both species having cationic functionality, they occupy different regions of surface rather than adsorb on top of each other.

within 24 h of preparation and stored in a refrigerator near 4 °C. The strain was originally a clinical isolate, and is today widely used in standardized tests of bacterial antibiotic susceptibility. This particular strain was chosen for its non-pathogenic behavior, while still closely resembling strains found in hospital infections.

Bacterial adhesion was studied in the same slit-flow chambers used to characterize nanoparticle deposition and backfill. The chamber was oriented so the surface of interest was perpendicular to the floor, avoiding gravitational forces in the same direction as interfacial interactions between bacteria and the substrate. Then bacteria were flowed through the chamber at a wall shear rate of 22 s^{-1}, and their adhesion to the surface was monitored on video, focusing at the surface of the microscope slide. A wall shear rate near 20 s^{-1} was chosen to be gentle. (With the pump setting targeting 20 s^{-1}, an actual wall shear rate of 22 s^{-1} was determined, based on our measurement of the actual volumetric flow rate via the "bucket and stopwatch" method.) Subsequent analysis of video images, using Image J, produced data on the numbers of adherent bacteria as a function of time. While the same DI water and buffer concentration were always used for surface fabrication, ionic strength was systematically varied in bacterial adhesion studies.

Zeta potentials were measured using 1-micron silica microspheres (Geltech, Orlando) at a concentration of 100 ppm, onto which different amounts of nanoparticles and/or PLL–PEG were absorbed, in order to simulate collecting surfaces. Zeta potentials of the bacterial suspensions were also measured as a function of ionic strength.

3. Results

3.1. Surface fabrication and their characterization

Surfaces were created by depositing nanoparticles from flowing suspensions and backfilling the remaining surface area with a polymer brush. The first step, nanoparticle deposition, was demonstrated previously [21] and is addressed here in the Supporting Information. There it is shown that i) particle deposition is linear in time, allowing for controlled particle loadings on the surface and ii) reflectometry signal is proportional to the AFM-measured particle loadings. Also, cationic nanoparticle-functionalized silica surfaces have been found to be robust, with retention of nanoparticles after aggressive treatments including exposure to high and low ionic strengths, organic solvents, drying, and sonication.[21]

In making the composite surfaces, PLL–PEG was adsorbed following nanoparticle deposition. An example is shown in Fig. 2A, a reflectivity trace for nanoparticle deposition followed by backfilling. Here after ~5 min of nanoparticle deposition, the surface loading of nanoparticles is locked in by re-introduction of deionized (DI) water. Then, in preparation for polymer deposition, the solution is switched to pH 7.4 (I = 0.026 M) phosphate buffer, and then polymer is introduced at 100 ppm in the same buffer. The trace demonstrates that the nanoparticles are retained, prior to polymer introduction, and that the net interfacial mass increases upon polymer introduction. The transport-limited rate of polymer adsorption, starting around

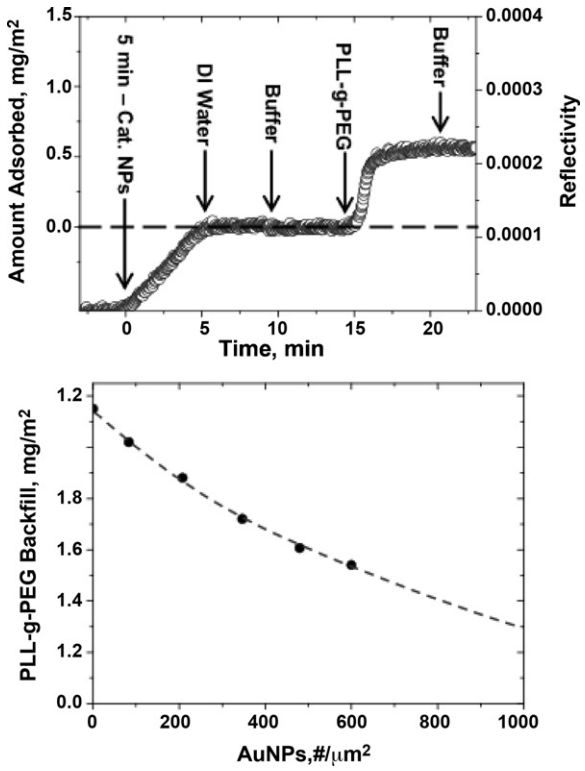

Fig. 2. Evidence for exclusion of PLL–PEG backfill by cationic nanoparticles. (A) adsorption sequence for nanoparticles followed by rinsing and exposure to PLL–PEG solutions. The adsorbed amount of PLL–PEG is based on the calibration for polymer coverage and does not apply to the nanoparticle deposition portion of the experiment. (B) Summary of PLL–PEG backfill amounts as a function of the amount of nanoparticles previously deposited.

15 min, is identical to that on bare silica, suggesting that nanoparticles are not being displaced by the copolymer, and that instead the copolymer is adhering to bare regions of the silica. An "exchange reaction" in which adsorbing polymer displaces nanoparticles would exhibit a slower net increase in mass due to loss of nanoparticles during polymer adsorption. A reduction in signal might be equally likely for nanoparticle removal.

With a PLL–PEG coverage of 1.1 mg/m^2 on silica containing no nanoparticles, the lower PLL–PEG coverage on a nanoparticle-containing surface in Fig. 2A suggests the adsorption of the PLL–PEG to backfill only the bare silica. Fig. 2B provides additional evidence: The adsorbed amount of PLL–PEG is summarized as a function of nanoparticle coverage. Surfaces with more nanoparticles accommodate less polymeric backfill, demonstrating the exclusion of the PLL–PEG by cationic nanoparticles. Further evidence for the compatibility of nanoparticles and PLL–PEG is found in the Supporting Information. There, micrographs reveal retention of particles after backfilling, with no evidence of particle rearrangement. There is also a slight reduction in the apparent particle height via AFM, as a result of the polymer adsorbing around the particles, consistent with a lack of polymer adsorption on the nanoparticles. As explained in the Supporting Information, with backfill polymer dried down between the nanoparticles, the distance between the tops of nanoparticles and the substrate is reduced about a nanometer.

Table 1 summarizes zeta potentials for surfaces with nanoparticle contents relevant to the bacterial adhesion studies. In particular, the nanoparticle loadings of 275 and 1000/um^2 correspond to near-threshold (defined below in terms of bacterial adhesion) and fully loaded surfaces, respectively. (Maximum loading describes our ability to deposit the nanoparticles, also discussed below, as opposed to a tightly packed nanoparticle arrangement.) As is well-known, the silica substrate is substantially negative at the pH 7.4 of this study, with details depending on ionic strength. Our data confirm the literature [33]. A saturated layer of the PLL–PEG brush (1.1 mg/m^2), while reducing the magnitude of this negative surface potential, does not change the sign of the surface charge. This occurs for 2 reasons: First, the amount of PLL at the base of the PLL–PEG brush (0.15 mg/m^2 compared with 0.4 mg/m^2 in a saturated PLL layer) is insufficient to neutralize the negative silica charge. Additionally, perturbation of the shear plane by the brush still allows some access to the surface charge, even for $\kappa^{-1} = 1$ nm. While we have previously estimated brush heights of 8–9 nm[22] using an Alexander-De Gennes treatment for the brush [34,35], this approximation assumes that the tethers are completely non-adsorbing. The observation of PEG adsorption onto silica [36,37], combined with a demonstration of how such adsorption at the base of the brush reduces the length and density of the tethers [38], suggests our brushes might be thinner than the equivalent 8–9 nm step-function height estimate or that the hydrodynamic field may penetrate more deeply into the outer region of the brush than originally anticipated.

Also in Table 1, a saturated layer of PLL produces a slightly positive surface charge at all ionic strengths. This is not true of a "full" layer of nanoparticles where the net zeta potentials of the surface are −41 to −51 mV. This suggests that despite the strong positive zeta potentials of the cationic nanoparticles in suspension (including 28 ± 3 mV in DI water), the maximum deposition coverage (in the Supporting Information, 1000 np/um^2) does not produce a packed nanoparticle layer, but instead leaves much bare silica. (Higher loadings can be achieved by increasing the ionic strength during nanoparticle deposition, but the surface is still far from "packed" with nanoparticles.) PLL–PEG backfilling around immobilized nanoparticles produces surfaces with net negative charge, not surprisingly.

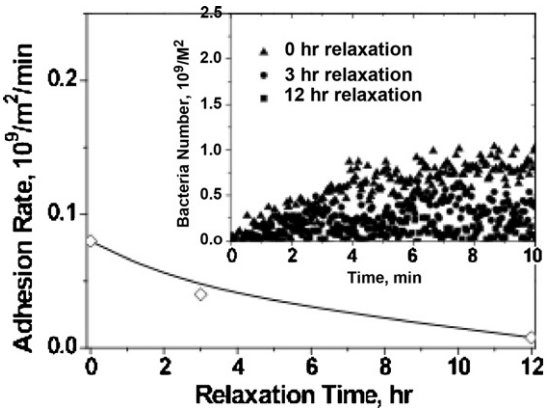

Fig. 3. Bacterial adhesion on an adsorbed PLL–PEG layer aged to different extents in DI water. Inset shows raw data while main graph summarizes coverages as a function of brush aging time.

3.2. Bacterial adhesion

Key to the adhesion and manipulation of bacteria using surface-immobilized nanoparticles is the elimination of bacterial interactions with the remaining surface area. Our surfaces are designed with the intention that PLL–PEG –covered areas should not adhere flowing bacteria. This was reported to be the case, or nearly so, for PLL–PEG layers with similar molecular weights and architectures as that of the copolymer employed here, exposed to *S. aureus* [8]. Further, the particular copolymer architecture and MW in our study was shown by others [31,32] and confirmed by us [22] to nearly completely resist protein adsorption. Fig. 3 demonstrates interesting bacterial adhesion, depending on the layer age after the relatively short adsorption period. Here, saturated adsorbed layers of PLL–PEG (containing no nanoparticles) are exposed to flowing suspensions of *S. aureus* (5×10^5/ml), after different aging times in flowing buffer. *S. aureus* adheres modestly on PLL–PEG layers shortly after their adsorption. However, bacterial adhesion decreases with the brush age (in buffer; no further polymer adsorbs) and is nearly completely eliminated after 12 h. Presumably slow relaxations in the polymer brush layer eliminate either loops of cationic backbone protruding from the newly formed brush or tiny bare spots on the surface, which are bacteria-adhesive. We see no such layer age dependence of the adsorption of several proteins: albumin, fibrinogen, and myoglobin [39]. These proteins do not adsorb onto freshly adsorbed brushes of the PLL–PEG copolymer. Because of the bacterial adhesion to fresh brushes, nanoparticle-containing surfaces, with their PLL–PEG brush backfill layers have all been allowed to relax in phosphate buffer for 12 h prior to exposure to flowing *S. aureus*.

Fig. 4A shows a series of kinetic runs for the capture of flowing *S. aureus* from pH 7.4 phosphate buffer with $I = 0.005$ M ($\kappa^{-1} = 4$ nm) onto a series of surfaces with increasing density of nanoparticles. Included is a trace for bacterial capture on a saturated PLL layer, which acts as a calibration of transport-limited capture. Here, the positive charge on the PLL layer (zeta potential of ~5 mV) renders these surfaces strongly and rapidly adherent to bacteria: *S. aureus* adheres at the transport-limited rate, as evidenced by a 1/3-wall shear rate dependence and a linear concentration dependence of the bacterial capture rate [40]. Since bacterial adhesion studies on the nanoparticle surfaces were done with different batches of bacteria on different days, with the bacterial concentration varying by up to a factor of 2 and difficult to quantify independently with sufficient precision, the transport-limited rate measured on PLL with each bacterial batch facilitated a calibration of relative concentration for different bacterial batches, enabling their comparison in the form of collection efficiencies.

Table 1
Zeta potentials, in mV, of silica particles with various surface layers.

	I = 0.10 M κ^{-1} = 1 nm	I = 0.026 M κ^{-1} = 2 nm	I = 0.005 M κ^{-1} = 4 nm
Bare silica	−57 ± 3	−73 ± 4	−85 ± 5
Saturated PLL–PEG, 1.1 mg/m^2	-17 ± 4	−26 ± 4	−30 ± 2
Saturated PLL, 0.4 mg/m^2	2 ± 4	6 ± 4	4 ± 4
Silica + 275 np/um^2	−53 ± 4	−72 ± 4	−81 ± 5
Silica + 1000 np/um^2	−41 ± 4	−46 ± 5	−51 ± 4
Silica + 275 np/um^2 + PLL–PEG backfill	−23 ± 3	−29 ± 4	−39 ± 4
Silica + 1000 np/um^2 + PLL–PEG backfill	−19 ± 5	−20 ± 4	−30 ± 3
Below are data for suspended items, not adsorbed to silica spheres			
S. aureus	−12 ± 3	−25 ± 3	−12 ± 2
Nanoparticles in suspension	5 ± 2	8 ± 3	9 ± 2

Key features of bacterial capture on nanoparticle-containing surfaces in Fig. 4A include the linearity with respect to time within each data set and the increase in capture with increased nanoparticle density. The former suggests that bacterial capture is controlled strictly by substrate-bacterial interactions without interactions between previously immobilized and incoming bacteria. Indeed at the transport-limited rate, after 10 min the surface area occupied by bacteria is only 0.4%.

Fig. 4B summarizes the dependence of the bacterial capture rate on the nanoparticle surface density for the data in Fig. 4A plus more at this and other ionic strengths. The Supporting Information provides examples of captured video frames for bacteria at 5 min of bacterial flow, for surfaces containing 0, 40, and 200 nanoparticles/um^2. These data demonstrate the isolated, random arrangement of the captured bacteria, but cannot provide information on viability or bacterial structure due to the wide field needed for bacterial counting. In all cases (not all data shown), bacterial capture are linear in time for at least the first 10 min of each run, similar to the examples in Fig. 4A. For all three ionic strengths in Fig. 4B, the bacterial adhesion rates increase with density of cationic patches, demonstrating the importance of electrostatic attractions to bacteria-surface interactions. At the greatest surface densities of cationic nanoparticles, bacterial capture rates on nanoparticle-functionalized surfaces approach the established transport-limited rate on an adsorbed PLL-layer. However, below 500 or 1000 nanoparticles/um^2, depending on the ionic strength, surface composition, rather than transport, controls bacterial adhesion.

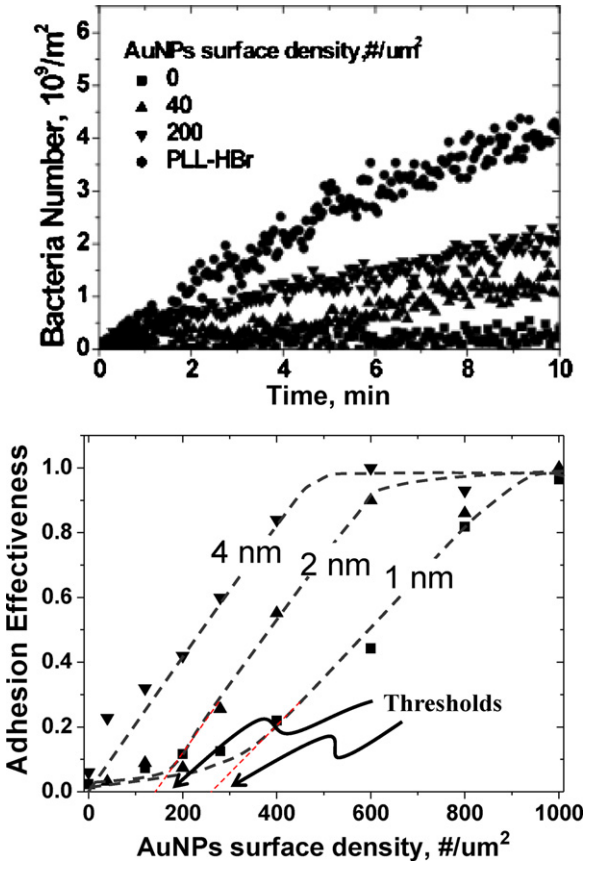

Fig. 4. *S. aureus* capture and accumulation on composite surfaces. Adhesion efficiency is relative to the transport-limited rate at a wall shear rate of 22 s^{-1}. (A) Raw data for a single batch, including the capture on a pre-adsorbed PLL layer to establish the batch-dependent transport-limited capture rate. Here the ionic strength is 0.005 M and the Debye length is 4 nm. (B) Summary of capture efficiencies as a function of nano-particle surface density for ionic strengths corresponding to the Debye lengths shown.

In the regime of surface-limited bacterial adhesion, the surfaces are substantially net negative, so that electrostatic and steric repulsions from the back-filled surface areas oppose bacterial capture. In this regime, bacterial capture is driven by attractions to the cationic nanoparticles, with the capture rate increasing monotonically with their surface density. Interestingly, at ionic strengths corresponding to a Debye length of 4 nm, the rate data pass through the origin and are linear in the nanoparticle density, while at κ^{-1} = 1 and 2 nm, the increase in bacterial capture rate occurs above a finite x-intercept. These data sets are roughly sigmoidal, and present an effective adhesion threshold, a density of nanoparticles required for substantial bacterial capture. Previously demonstrated sensitivity of thresholds to features of the analyte (other than bacteria) suggests the use of these surfaces in applications requiring sharply selective binding [27,39,41].

4. Discussion

While the thresholds for κ^{-1} = 1 and 2 nm in Fig. 4B are imperfect (i.e. there is a low level of bacterial capture below the thresholds, especially at κ^{-1} = 1 nm), their presence is significant: Thresholds indicate weak bacterial interactions with individual nanoparticles and the requirement of several nanoparticles for the capture of each bacterium, sometimes termed "multivalency" [25,41]. As the ionic strength is increased, the electrostatic attractions are progressively weakened, relative to the repulsion from the brush, and the threshold shifts further to the right towards greater surface loadings of nanoparticles.

At the other extreme with κ^{-1} = 4 nm, the electrostatic nanoparticle-bacterial attractions are stronger and longer range. It turns out that, for our particular system, at κ^{-1} = 4 nm, the electrostatic attractions are sufficiently strong that the adhesion threshold vanishes, and bacterial capture is no longer multivalent. Here, instead, individual immobilized nanoparticles are each sufficient to capture bacteria, and up to the point of transport-limited

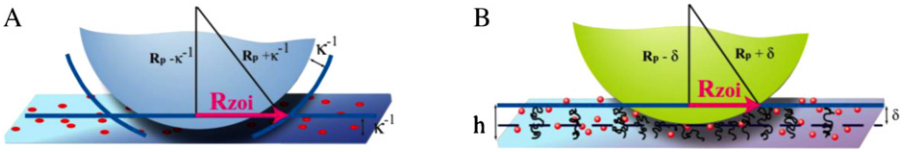

Fig. 5. Contact regions between (A) particles and electrostatic surfaces versus (B) bacteria and brush surfaces. For the brushy surface, the compression length, δ, is approximated here by the brush persistence length, ξ.

bacterial capture, the rate of bacterial capture is proportional to the nanoparticle loading on the substrate. Given the tiny dimensions of our nanoparticles, the ability of these materials to each individually capture and hold bacteria, even in gentle flow might be considered remarkable. In our studies here, without changes in ionic strength, pH, or flow conditions, the univalent bacterial capture was found to be irreversible.

Also worth mentioning, while cationic nanoparticles and polymers are generally classified as "antimicrobial," due to their potential to disrupt cell membranes, we have not determined if bacteria on our surfaces are viable. We suspect, however, that in the limit of single nanoparticle capture of bacteria (in the univalent limit, with surfaces containing very few nanoparticles) that the bacteria are minimally affected by a single point contact with a 10-nm nanoparticle. Future work will address the concentration and ionic strength conditions, if any, where our surfaces reduce bacterial viability. We note that in general there is an advantage to decouple adhesion and capture from biofunctionality: The placement of surface elements with completely independent functions (adhesion, selectivity, killing, or signaling) allows surfaces to be tuned precisely for applications of interest.

Interesting insights into the mechanisms of bacterial interactions and the role of electrostatic versus steric interactions can be gained by comparing bacterial capture in Fig. 4 to the capture of negative silica particles on negative silica surfaces decorated with either flat cationic polymer patches [25,27] or cationic nanoparticles [21,41]. Fig. 5 compares the surface structures [25,27,28], and an important parameter is the "zone of influence," an area on the collecting surface exerting repulsive forces on approaching particles. This contact area is roughly proportional to the total repulsion between the particles (or bacteria) and the collector. A proportionate number of attractive elements are needed, within the zone of influence, to produce particle capture. A prediction of the adhesion threshold follows from calculations of the probabilities of finding the appropriate numbers of randomly arranged cationic adhesion elements, for the silica sphere system [25].

In the silica sphere- silica flat system, the contact area was defined by the electrostatic repulsions [25]. From a geometrical analysis of the intersection of the double layer of the particle with a plate, we approximated $R_{zoi} = 2\sqrt{\kappa^{-1}a}$, with a being the particle radius. In the current system, the repulsive contact area is defined by the compressibility of the polymer brush. A bacteria's thermal energy gives the compressive force on the outer region of the brush (in the absence of attractive patches or particles), and brush compression defines the extent of bacterial-surface contact. In the Alexander-DeGennes brush model, the term "blob" describes a unit of a tether possessing a kT of energy [34,35]. Blob size or brush persistence length, ξ, is equal to the tether spacing and, for our system using a first approximation of non-adsorbing PEG chains, $\xi \sim 2$ nm. Then the radius of the contact area between a bacterium and the brush is $R_{zoi} = 2\sqrt{\xi a} = 63$ nm. This is similar in range to R_{zoi} at an ionic strength of 0.026 M, in the silica sphere – silica surface system.

In the silica sphere – silica flat system, the effect of ionic strength on the zone of influence is dominant in establishing the adhesion thresholds [25]. In the bacteria–brush system, ionic strength affects the strength of the adhesive elements but not the repulsive contact area. Therefore, the bacterial adhesion thresholds increase with decreasing Debye length, while in the silica sphere system, the opposite occurs.

It is tempting to quantify the relative nanoparticle heights and brush protrusion. While we can say the expected brush heights (treating the brush as a step function) are 8–9 nm or slightly less with PEG adsorption onto silica, and that the dry nanoparticle heights by AFM are 7–8 nm, the resolution necessary (nanometer to sub-nanometer) to describe the relative brush and nanoparticle height in buffer is not experimentally accessible. Hydrodynamic, scattering, and electrokinetic measures of brush height (the latter relative to electrostatic interactions) do not adequately anticipate the forces experienced by flowing bacteria. The actual compressibility of a brush by a bacterium, with the nanometer resolution achieved by variations in Debye length from 1–2 nm, is very sensitive to the fine structure of the outer brush edge and is not known for our system, which is thin relative to model brushes probed by neutron methods [38]. Likewise restructuring of the ligand shell on the nanoparticles between wet and dry (AFM) states could easily produce height differences, between the wet and dry states, of 1–3 nm. Even with this uncertainty, however, we can say, from the observations here, that the nanoparticles are mostly inaccessible to approaching bacteria, obstructed by the outer structure of the PEG brush. The exception occurs at $\kappa^{-1} = 4$ nm when the nanoparticle double layer protrudes from the brush and facilitates substantial bacterial capture. The observed variation in bacterial capture in the range $\kappa^{-1} = 1$–4 nm fall well within expectations for 9 nm brushes and nanoparticles with 7 nm cores and 1–2 nm thick ligand shells.

A final point is the observation of the affect of brush age on bacterial adhesion. While it has been documented that the most biocompatible adsorbed brushes require long adsorption periods to increase the surface mass [42] (we agree that the penetration of the final brushes into a growing brush is a slow process), our observation is that this aging period is necessary for reasons of relaxation rather than increasing the surface mass. Our brushes were aged in DI water rather than in a solution of the adsorbing polymer, so that the interfacial mass could not increase during the aging period. Notably, bacterial adhesion onto these brushes is nonlinear in time. The leveling off of bacterial capture in Fig. 4 may indicate a finite number of interfacial defects that dissipate as the adsorbed polymer relaxes.

5. Conclusions

This work demonstrates how immobilized nanoparticles on biocompatible brushy surfaces provide material interfaces useful for the manipulation of bacterial attachment. Adhesion of bacteria to immobilized nanoparticles is opposed by steric repulsions from a hydrated PEG, whose height is similar to or slightly larger than the nanoparticle size. At large Debye lengths, electrostatic attractions between the cationic nanoparticles and the approaching bacteria sufficiently exceed the range of steric repulsions from the brush, causing bacteria to adhere strongly to the surface. At sparse nanoparticle loadings on the surface, for $\kappa^{-1} = 4$ nm bacteria can be captured by individual nanoparticles (univalent capture). Conversely at small Debye lengths, the range of electrostatics is shortened such that the effective binding energy between individual nanoparticles and bacteria is insufficient to capture the

bacteria from gentle shearing flow. At these conditions, when the surface is sufficiently loaded in nanoparticles, bacteria contacting multiple nanoparticles are captured. This binding mechanism, termed "multivalent" is typified by a threshold in the surface loading of nanoparticles needed for appreciable bacterial capture. In this way this paper has demonstrated the use of ionic strength to tune the mechanism for bacterial capture from univalent to multivalent.

The work also documented that relaxations in PEG–PLL graft copolymers on silica surfaces act, at constant interfacial mass, to increase the biocompatibility and bacterial resistance of these surfaces, over a timescale of several hours.

Acknowledgements

This work was made possible by grants from NSF, DMR-0805061, CBET 0932719 and the UMass Center for Hierarchical Manufacturing.

Appendix A. Supplementary data

Supplementary data associated with this article can be found, in the online version, at doi:10.1016/j.colsurfb.2011.05.010.

References

[1] K.D. Park, Y.S. Kim, D.K. Han, Y.H. Kim, E.H.B. Lee, H. Suh, K.S. Choi, Biomaterials 19 (1998) 851–859.
[2] N.P. Desai, S.F.A. Hossainy, J.A. Hubbell, Biomaterials 13 (1992) 417–420.
[3] A. Shimotoyodome, T. Koudate, H. Kobayashi, J. Nakamura, I. Tokimitsu, T. Hase, T. Inoue, T. Matsukubo, Y. Takaesu, Antimicrob. Agents Chemother 51 (2007) 3634–3641.
[4] S.H. Hsu, C.M. Tang, C.C. Lin, Biomaterials 25 (2004) 5593–5601.
[5] F. Boulmedais, B. Frisch, O. Etienne, P. Lavalle, C. Picart, J. Ogier, J.C. Voegel, P. Schaaf, C. Egles, Biomaterials 25 (2004) 2003–2011.
[6] P. Kingshott, J. Wei, D. Bagge-Ravn, N. Gadegaard, L. Gram, Langmuir 19 (2003) 6912–6921.
[7] R.R. Maddikeri, S. Tosatti, M. Schuler, S. Chessari, M. Textor, R.G. Richards, L.G. Harris, J. Biomed. Mater. Res. Part A 84A (2008) 425–435.
[8] L.G. Harris, S. Tosatti, M. Wieland, M. Textor, R.G. Richards, Biomaterials 25 (2004) 4135–4148.
[9] A. Razatos, Y.L. Ong, F. Boulay, D.L. Elbert, J.A. Hubbell, M.M. Sharma, G. Georgiou, Langmuir 16 (2000) 9155–9158.
[10] L.K. Ista, H.Y. Fan, O. Baca, G.P. Lopez, FEMS Microbiol. Lett. 142 (1996) 59–63.
[11] R. Muller, S. Ruhl, K.A. Hiller, G. Schmalz, H. Schweikl, J. Biomed. Mater. Res. Part A 84A (2008) 817–827.
[12] M. Paulsson, M. Kober, C. Freijlarsson, M. Stollenwerk, B. Wesslen, A. Ljungh, Biomaterials 14 (1993) 845–855.
[13] A. Roosjen, H.C. van der Mei, H.J. Busscher, W. Norde, Langmuir 20 (2004) 10949–10955.
[14] I.C.S. Fernandez, H.C. van der Mei, S. Metzger, D.W. Grainger, A.F. Engelsman, M.R. Nejadnik, H.J. Busscher, Acta Biomater. 6 (2010) 1119–1124.
[15] G. Subbiahdoss, B. Pidhatika, G. Coullerez, M. Charnley, R. Kuijer, H.C. van der Mei, M. Textor, H.J. Busscher, Eur. Cells Mater. 19 (2010) 205–213.
[16] R. Muller, A. Eidt, K.A. Hiller, V. Katzur, M. Subat, H. Schweikl, S. Imazato, S. Ruhl, G. Schmalz, Biomaterials 30 (2009) 4921–4929.
[17] B. Zdyrko, V. Klep, X.W. Li, Q. Kang, S. Minko, X.J. Wen, I. Luzinov, Mater. Sci. Eng. C-Biomimetic Supramol. Syst. 29 (2009) 680–684.
[18] C.H. Choi, J.H. Lee, T.S. Hwang, C.S. Lee, Y.G. Kim, Y.H. Yang, K.M. Huh, Macromol. Res. 18 (2010) 254–259.
[19] H.W. Shim, J.H. Lee, B.Y. Kim, Y.A. Son, C.S. Lee, J. Nanosci. Nanotechnol. 9 (2009) 1204–1209.
[20] P. Krsko, J.B. Kaplan, M. Libera, Acta Biomater. 5 (2009) 589–596.
[21] J. Zhang, S. Srivastava, R. Duffadar, J.M. Davis, V.M. Rotello, M.M. Santore, Langmuir 24 (2008) 6404–6408.
[22] S. Gon, M. Bendersky, J.L. Ross, M.M. Santore, Langmuir 26 (2010) 12147–12154.
[23] P. Francois, P. Vaudaux, T.J. Foster, D.P. Lew, Infect. Control Hosp. Epidemiol. 17 (1996) 514–520.
[24] D.J. Stickler, R.J.C. McLean, Cells Mater. 5 (1995) 167–182.
[25] R. Duffadar, S. Kalasin, J.M. Davis, M.M. Santore, J. Colloid Interface Sci. 337 (2009) 396–407.
[26] S. Kalasin, M.M. Santore, Langmuir 26 (2010) 2317–2324.
[27] M.M. Santore, N. Kozlova, Langmuir 23 (2007) 4782–4791.
[28] S. Kalasin, S. Martwiset, E.B. Coughlin, M.M. Santore, Langmuir 26 (2010) 16865–16870.
[29] S. Srivastava, B. Samanta, B.J. Jordan, R. Hong, Q. Xiao, M.T. Tuominen, V.M. Rotello, J. Am. Chem. Soc. 129 (2007) 11776–11780.
[30] T. Teranishi, S. Hasegawa, T. Shimizu, M. Miyake, Adv. Mater. 13 (2001) 1699–1701.
[31] G.L. Kenausis, J. Voros, D.L. Elbert, N.P. Huang, R. Hofer, L. Ruiz-Taylor, M. Textor, J.A. Hubbell, N.D. Spencer, J. Phys. Chem. B 104 (2000) 3298–3309.
[32] N.P. Huang, R. Michel, J. Voros, M. Textor, R. Hofer, A. Rossi, D.L. Elbert, J.A. Hubbell, N.D. Spencer, Langmuir 17 (2001) 489–498.
[33] P.J. Scales, F. Grieser, T.W. Healy, L.R. White, D.Y.C. Chan, Langmuir 8 (1992) 965–974.
[34] S. Alexander, J. Phys. (Paris) 38 (1977) 977.
[35] P.G. de Gennes, J. Phys. (Paris) 38 (1976) 1443.
[36] Z.G. Fu, M.M. Santore, Colloid Surf. A-Physicochem. Eng. Aspects 135 (1998) 63–75.
[37] Z.L. Fu, M. Santore, Macromolecules 32 (1999) 1939–1948.
[38] M.S. Kent, Macromol. Rapid Commun. 21 (2000) 243–270.
[39] S. Gon, M.M. Santore, Langmuir 27 (2011) 1487–1493.
[40] S. Kalasin, J. Dabkowski, K. Nusslein, M.M. Santore, Colloid Surf. B-Biointerfaces 76 (2010) 489–495.
[41] M.M. Santore, J. Zhang, S. Srivastava, V.M. Rotello, Langmuir 25 (2009) 84–96.
[42] J.L. Dalsin, L.J. Lin, S. Tosatti, J. Voros, M. Textor, P.B. Messersmith, Langmuir 21 (2005) 640–646.